electronics

MDPI

Article

Effects of Active Layer Thickness on the Electrical Characteristics and Stability of High-Mobility Amorphous Indium–Gallium–Tin Oxide Thin-Film Transistors

Dae-Hwan Kim †, Hyun-Seok Cha †, Hwan-Seok Jeong, Seong-Hyun Hwang and Hyuck-In Kwon *

School of Electrical and Electronics Engineering, Chung-Ang University, Seoul 06974, Korea; pccdhkim@naver.com (D.-H.K.); ckgustjr0803@naver.com (H.-S.C.); hwanseok518@naver.com (H.-S.J.); ajttjdwlsgus@naver.com (S.-H.H.)

* Correspondence: hyuckin@cau.ac.kr; Tel.: +82-2-820-5293

† Co-first author, these authors contributed equally to this work.

Abstract: Herein, we investigated the effects of active layer thickness (t_S) on the electrical characteristics and stability of high-mobility indium–gallium–tin oxide (IGTO) thin-film transistors (TFTs). IGTO TFTs, with t_S values of 7 nm, 15 nm, 25 nm, 35 nm, and 50 nm, were prepared for this analysis. The drain current was only slightly modulated by the gate-to-source voltage, in the case of the IGTO TFT with t_S = 50 nm. Under positive bias stress (PBS), the electrical stability of the IGTO TFTs with a t_S less than 35 nm improved as the t_S increased. However, the negative bias illumination stress (NBIS) stability of these IGTO TFTs deteriorated as the t_S increased. To explain these phenomena, we compared the O1s spectra of IGTO thin films with different t_S values, acquired using X-ray photoelectron spectroscopy. The characterization results revealed that the better PBS stability, and the low NBIS stability, of the IGTO TFTs with thicker active layers were mainly due to a decrease in the number of hydroxyl groups and an increase in the number of oxygen vacancies in the IGTO thin films with an increase in t_S, respectively. Among the IGTO TFTs with different t_S, the IGTO TFT with a 15-nm thick active layer exhibited the best electrical characteristics with a field-effect mobility (μ_{FE}) of 26.5 $cm^2/V{\cdot}s$, a subthreshold swing (SS) of 0.16 V/dec, and a threshold voltage (V_{TH}) of 0.3 V. Moreover, the device exhibited robust stability under PBS (ΔV_{TH} = 0.9 V) and NBIS (ΔV_{TH} = −1.87 V).

Keywords: IGTO TFT; active layer thickness; positive bias stress stability; negative bias illumination stress stability

Citation: Kim, D.-H.; Cha, H.-S.; Jeong, H.-S.; Hwang, S.-H.; Kwon, H.-I. Effects of Active Layer Thickness on the Electrical Characteristics and Stability of High-Mobility Amorphous Indium–Gallium–Tin Oxide Thin-Film Transistors. *Electronics* **2021**, *10*, 1295. https://doi.org/10.3390/electronics10111295

Academic Editor: Matteo Meneghini

Received: 22 April 2021
Accepted: 27 May 2021
Published: 28 May 2021

Publisher's Note: MDPI stays neutral with regard to jurisdictional claims in published maps and institutional affiliations.

Copyright: © 2021 by the authors. Licensee MDPI, Basel, Switzerland. This article is an open access article distributed under the terms and conditions of the Creative Commons Attribution (CC BY) license (https://creativecommons.org/licenses/by/4.0/).

1. Introduction

Amorphous indium–gallium–zinc oxide (IGZO) thin-film transistors (TFTs) were reported for the first time by Nomura et al. in 2004; since, they have attracted significant attention because of their excellent electrical properties, low process temperature, large-area uniformity, and low fabrication cost [1–5]. Currently, IGZO TFTs are being widely used as a backplane for large-area active-matrix flat-panel displays, such as organic light-emitting diode (OLED) displays and liquid-crystal displays (LCD) [6–8]. The recent development of low-temperature polysilicon oxide technology is expected to further expand the application range of IGZO TFTs in the field of displays [7,8]. However, the relatively low field-effect mobility of IGZO TFTs (μ_{FE} = ~10 $cm^2/V{\cdot}s$) still hinders their application in the backplane of ultra-high-resolution and high-frame-rate displays [9,10]. This is because the OLED pixels require a high current to emit light. Therefore, the study presents a new low-voltage driving OLED pixel circuit with high-mobility amorphous oxide TFTs as the driving device with high resolution [11]. To date, various oxide semiconductors have been studied as active materials for high-mobility oxide TFTs [12–14]. Among them, IGTO has recently attracted considerable attention as a promising active material for next-generation high-mobility oxide TFTs. The In^{3+} and Sn^{4+} ions have almost similar electronic

structures. They have a small effective electron mass due to the 5 s orbital overlapping structure, leading to a highly conductive path for electron carriers, and remarkably high mobility [15,16]. Furthermore, the IGTO TFTs exhibit excellent electrical characteristics, even at low annealing temperatures (below 200 °C) [17–19].

For oxide TFTs, active layer thickness (t_S) is an important parameter that strongly affects the electrical performance and stability of these TFTs. To date, extensive research has been performed to determine the effects of t_S on the electrical characteristics and stability of oxide TFTs comprising different active materials. However, previous studies have reported different results for the effects of t_S on the electrical characteristics and stability of oxide TFTs according to the type of active material and fabrication process conditions. For example, Cho et al. [20] and Yang et al. [21] reported that the positive bias stress (PBS) stability of indium–zinc-oxide and IGZO TFTs deteriorated with an increase in t_S, respectively. Nevertheless, Lee et al. [22] and Li et al. [23] observed an improvement in the PBS stability of IGZO TFTs with an increase in t_S. These results imply that investigating the effects of t_S on the electrical performance and stability of IGTO TFTs is extremely necessary to determine the optimal t_S for IGTO TFTs. In this study, we examined the effects of t_S on the electrical characteristics and stability of IGTO TFTs. IGTO TFTs, with the t_S values of 7 nm, 15 nm, 25 nm, 35 nm, and 50 nm, were prepared for this analysis. A systematic study was conducted to investigate the physical mechanisms responsible for the observed effects of t_S on the electrical performance and PBS/NBIS stability of IGTO TFTs.

2. Materials and Methods

Figure 1a,b shows the schematic and top-view optical image of the fabricated IGTO TFTs, respectively. The IGTO TFTs were constructed on a heavily doped p-type Si wafer (resistivity < 0.005 Ω·cm) covered by 100-nm thick thermally grown SiO_2. The heavily doped p-type Si wafer was used as a substrate and a gate electrode. Thermally grown SiO_2 was used as a gate dielectric. IGTO active layers with the thicknesses of 7 nm, 15 nm, 25 nm, 35 nm, and 52 nm were deposited on the substrate by direct current magnetron sputtering under the following conditions: working pressure, 3.0 mTorr, Ar/O_2; gas mixing ratio, 21/9 sccm; sputtering power, 150 W; and chuck temperature, room temperature (RT). Then, a 100-nm thick indium–tin-oxide layer was deposited on the IGTO active layer-coated substrate to prepare source and drain electrodes of the TFTs. Subsequently, a 30-nm thick Al_2O_3 thin film was deposited as a passivation layer on top of the resulting substrate using radio frequency magnetron sputtering at RT. Finally, the IGTO TFTs were thermally annealed on a hot plate at 200 °C for 2 h in ambient air.

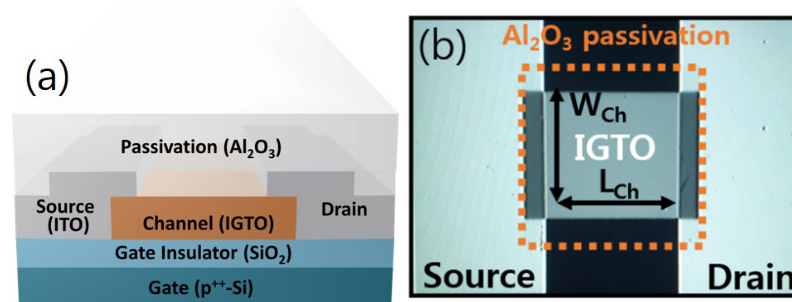

Figure 1. (**a**) Schematic and (**b**) top-view optical image of the fabricated IGTO TFTs.

The active, source/drain electrodes, and passivation layers were patterned using photolithography and a lift-off process. Electrical characteristics and stability of the IGTO TFTs were measured using a semiconductor parameter analyzer (4156C, Agilent Technologies, Santa Clara, CA, USA) at RT in ambient air. Crystalline structure of the IGTO thin films was analyzed using X-ray diffraction (XRD, New D8-Advance, Bruker-AXS, Wisconsin, USA) with CuKα radiation (λ = 0.15406 nm). Chemical properties of the IGTO thin films with different t_S were examined using X-ray photoelectron spectroscopy (XPS, K-alpha+,

Thermo Fisher Scientific-KR, Seoul, Korea). An Ar ion beam was employed to sputter the Al_2O_3 and IGTO thin films before XPS characterization.

3. Results and Discussion

Figure 2 shows the XRD patterns of a 35-nm thick IGTO thin film fabricated on an aluminosilicate glass substrate. The XRD pattern demonstrates only halo peaks at approximately 23° and 45°, originating from the glass substrate [24]. The results shown in Figure 2 indicate that the IGTO thin film has an amorphous phase, which is consistent with the results of previous studies [17].

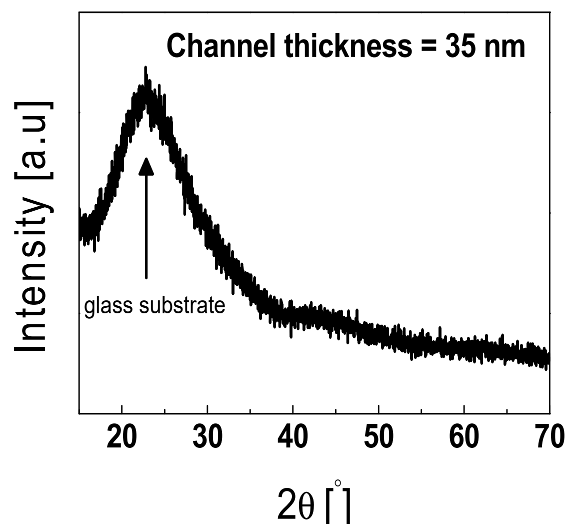

Figure 2. XRD pattern of the 35-nm thick IGTO thin film formed on the aluminosilicate glass substrate.

Figure 3 shows a semi-logarithmic scale plot of transfer curves for the IGTO TFTs (width/length (W/L) = 500 μm/500 μm), with the t_S of 7, 15, 25, 35, and 50 nm. Herein, the drain current (I_D) of all of the IGTO TFTs was evaluated by varying the gate-to-source voltage (V_{GS}) from −20 to 20 V at a fixed drain-to-source voltage (V_{DS}) of 1 V. Figure 3 shows that the I_D of the IGTO TFT with a t_S of 50 nm is slightly modulated by V_{GS}; therefore, the electrical characteristics and stability of only the IGTO TFTs with the t_S of 7, 15, 25, and 35 nm were examined in this study. Table 1 presents the electrical parameters of the IGTO TFTs with the t_S of 7, 15, 25, and 35 nm. The μ_{FE} was calculated using the maximum value of transconductance, and the V_{TH} was determined as the V_{GS} value causing $I_D = W/L \times 10^{-8}$ (A) at a V_{DS} of 1 V. The subthreshold swing (SS) was extracted as the $d(V_{GS})/d(\log I_D)$ value in the range of 10^{-10} A < I_D < 10^{-9} A. The V_{TH} decreased and the SS and the off-current (I_{OFF}) increased with an increase in t_S (Figure 3 and Table 1). The IGTO TFT with the t_S of 7 nm exhibited a significantly smaller μ_{FE} than those of the IGTO TFTs with thicker active layers. However, the μ_{FE} of the IGTO TFTs with a t_S larger than 15 nm only slightly increased with an increase in t_S. The results shown in Figure 3 and Table 1 are consistent with those reported in previous studies for oxide TFTs, and they demonstrate that t_S significantly affects the transfer characteristics of IGTO TFTs [25]. The negatively shifted V_{TH} and the large SS for the thick active oxide TFTs have been mainly attributed to the large number of free electrons within the oxide semiconductor and the higher sheet trap density in the active layer, respectively [26–28]. The increase in I_{OFF} with an increase in t_S was considered to be due to enhanced bulk conduction through the back-active layer [27]. The increase in μ_{FE} with an increase in t_S has been primarily ascribed to the reduced surface roughness scattering in the oxide semiconductor. As the carrier transport layer is farther from the surface of the thick film, the effect of the surface roughness on the carrier mobility is weaker in the thick film, compared with the thin film [29,30].

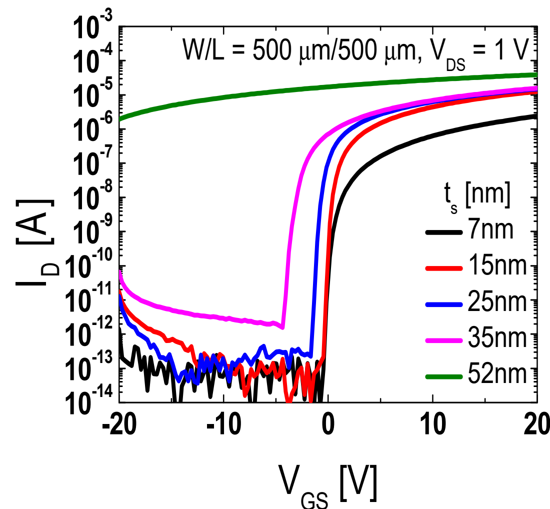

Figure 3. Semi-logarithmic scale plot of the transfer curves for the IGTO TFTs (W/L = 500 μm/500 μm) with the t_S of 7, 15, 25, 35, and 50 nm. I_D of all IGTO TFTs was measured by varying V_{GS} from −20 to 20 V at a fixed V_{DS} of 1 V.

Table 1. Electrical parameters of IGTO TFTs with the t_S of 7, 15, 25, and 35 nm.

t_S [nm]	V_{TH} [V]	μ_{FE} [cm^2·V^{-1}·S^{-1}]	SS [V/decade]	I_{OFF} [A]
7	1.3	6.5	0.16	5.75×10^{-14}
15	0.3	26.5	0.16	2.16×10^{-13}
25	−0.7	26.9	0.20	1.94×10^{-13}
35	−3.1	27.8	0.31	2.91×10^{-12}

Figure 4a–d shows the time dependence of the transfer curves for the IGTO TFTs with the t_S of 7, 15, 25, and 35 nm, respectively, at a V_{OV} ($V_{OV} = V_{GS} - V_{TH}$) of 20 V and a V_{DS} of 0 V. For every IGTO TFT, the transfer curves shifted in the positive direction with an increase in the stress time. The largest shift in V_{TH} (ΔV_{TH}) was observed for the IGTO TFT with the t_S of 7 nm (ΔV_{TH} = 3.1 V after stress for 3000 s), whereas the smallest ΔV_{TH} was noticed for the IGTO TFT with the t_S of 35 nm (ΔV_{TH} = 0.5 V after stress for 3000 s). Figure 4e depicts the ΔV_{TH} for the IGTO TFTs with different t_S under PBS at different stress times. Clearly, the magnitude of ΔV_{TH} for the fabricated IGTO TFTs decreased with an increase in t_S under PBS (Figure 4).

Figure 5a–d shows the time dependence of the transfer curves for the IGTO TFTs with the t_S of 7, 15, 25, and 35 nm, respectively, at a V_{OV} of −20 V and a V_{DS} of 0 V, under illumination using a white light-emitting diode (LED, wavelength 420–780 nm) backplane unit with a luminance of 2000 lux. For every IGTO TFT, the transfer curves shifted in the negative direction with an increase in the stress time. The largest magnitude of ΔV_{TH} was obtained for the IGTO TFT with the t_S of 35 nm (ΔV_{TH} = −11.2 V after stress for 3000 s), whereas the smallest magnitude of ΔV_{TH} was achieved for the IGTO TFT with the t_S of 7 nm (ΔV_{TH} = −0.6 V after stress for 3000 s). Figure 5e depicts the ΔV_{TH} for the IGTO TFTs with different t_S under negative bias illumination stress (NBIS) at different stress times. The magnitude of ΔV_{TH} for the fabricated IGTO TFTs increased with an increase in t_S under NBIS (Figure 5).

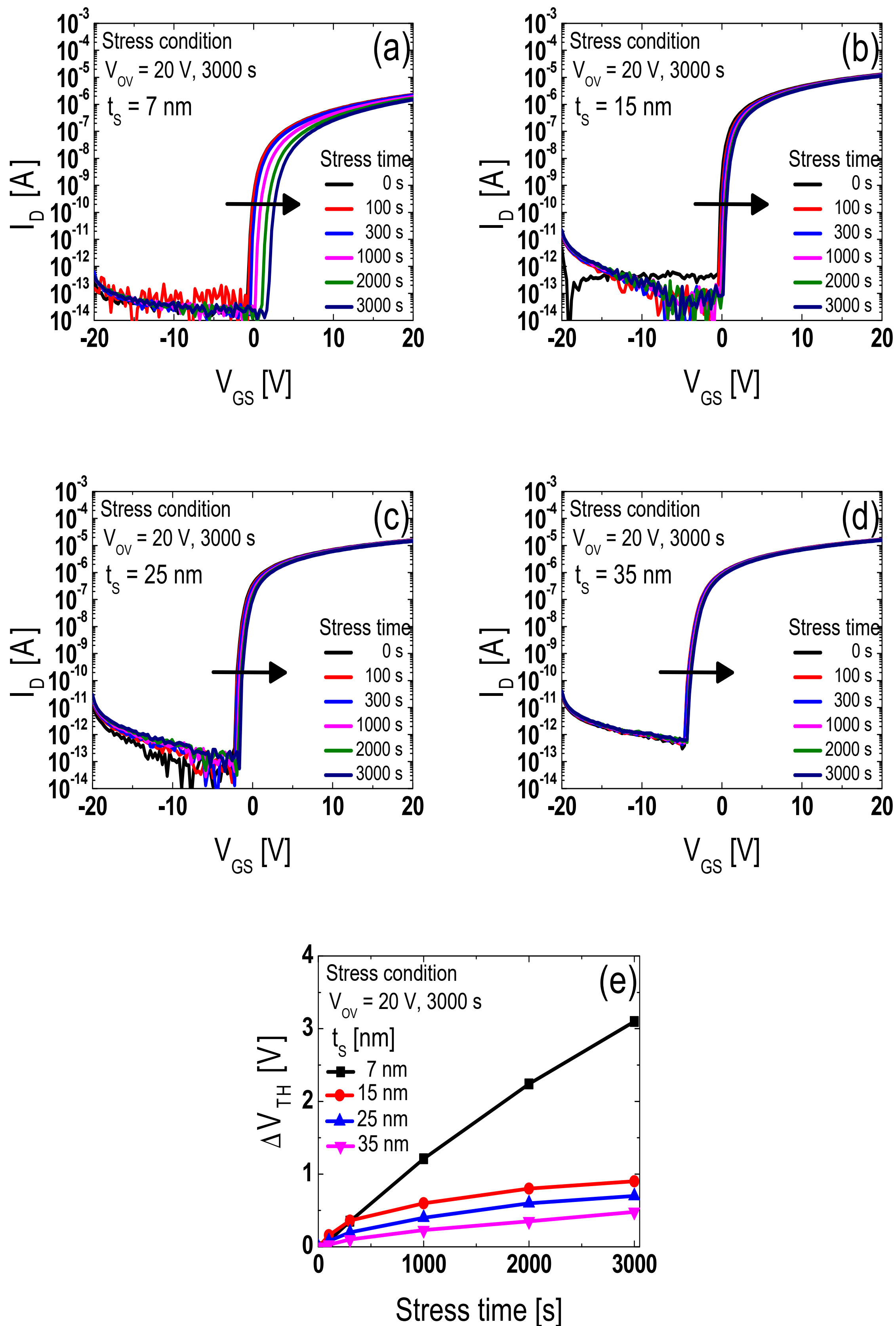

Figure 4. Time dependence of the transfer curves for IGTO TFTs with the t_S of (**a**) 7 nm, (**b**) 15 nm, (**c**) 25 nm, and (**d**) 35 nm at a constant V_{OV} of 20 V; (**e**) ΔV_{TH} for the IGTO TFTs with different t_S under PBS at different stress times.

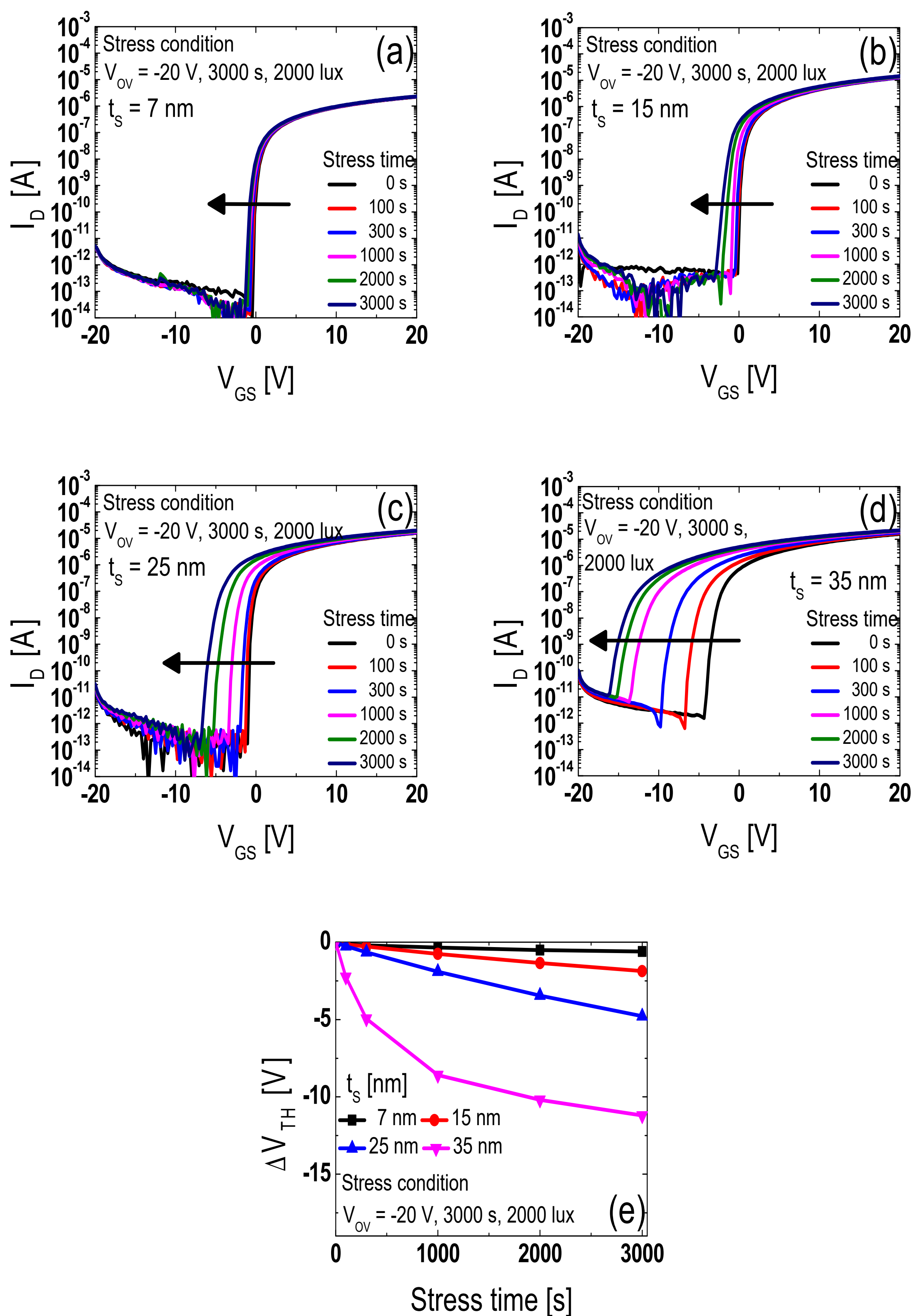

Figure 5. Time dependence of the transfer curves for the IGTO TFTs with the t_S of (**a**) 7 nm, (**b**) 15 nm, (**c**) 25 nm, and (**d**) 35 nm at a constant V_{OV} of −20 V under illumination using a light-emitting diode backplane unit with a luminance of 2000 lux; (**e**) ΔV_{TH} for the IGTO TFTs with different t_S under NBIS at different stress times.

To investigate the physical mechanisms responsible for the effects of t_S on the PBS and NBIS stability of IGTO TFTs (Figures 4 and 5), we characterized the *O*1*s* spectra of the IGTO thin films with different t_S obtained using XPS. Figure 6a–d shows the XPS *O*1*s* spectra of 7, 15, 25, and 35-nm thick IGTO thin films located near the IGTO/SiO_2 interface. The XPS *O*1*s* spectra were resolved into three sub-peaks originating from fully coordinated metal ions (metal–oxygen lattice (O_{Latt})), oxygen vacancies (O_{Vac}), and impurity-related oxygen (O_{Imp}). The XPS peak positions assigned to these sub-peaks were 530.0 eV (O_{Latt}), 531.0 eV (O_{Vac}), and 532.5 eV (O_{Imp}), respectively [14,17]. Figure 7 shows the relative peak area ratios of O_{Latt}, O_{Vac}, and O_{Imp} for the IGTO thin films with different t_S, located near the IGTO/SiO_2 interface. The relative peak area ratio of O_{Imp} was highest for the 7-nm thick IGTO thin film, and decreased with an increase in t_S (Figure 7). In previously reported studies on IGZO or IGTO TFTs, O_{Imp} was mainly ascribed to the O bond in the hydroxyl group (OH) [17]. The OH creates acceptor-like trap states close to the conduction band (CB) edge and accelerates the electron trapping process under PBS because of its polar nature [17,31–34]. Considering this, the lower PBS stability of the IGTO TFTs with thinner active layers can be ascribed to the high concentration of OH in the channel layer. It has been reported that a thicker active layer can isolate the channel from ambient factors, including H_2O molecules, even after the passivation layer is deposited on the active layer [35]. Effective self-passivation from H_2O molecules in the air is the most probable reason for the better PBS stability of the IGTO TFTs with thicker active layers (Figure 7).

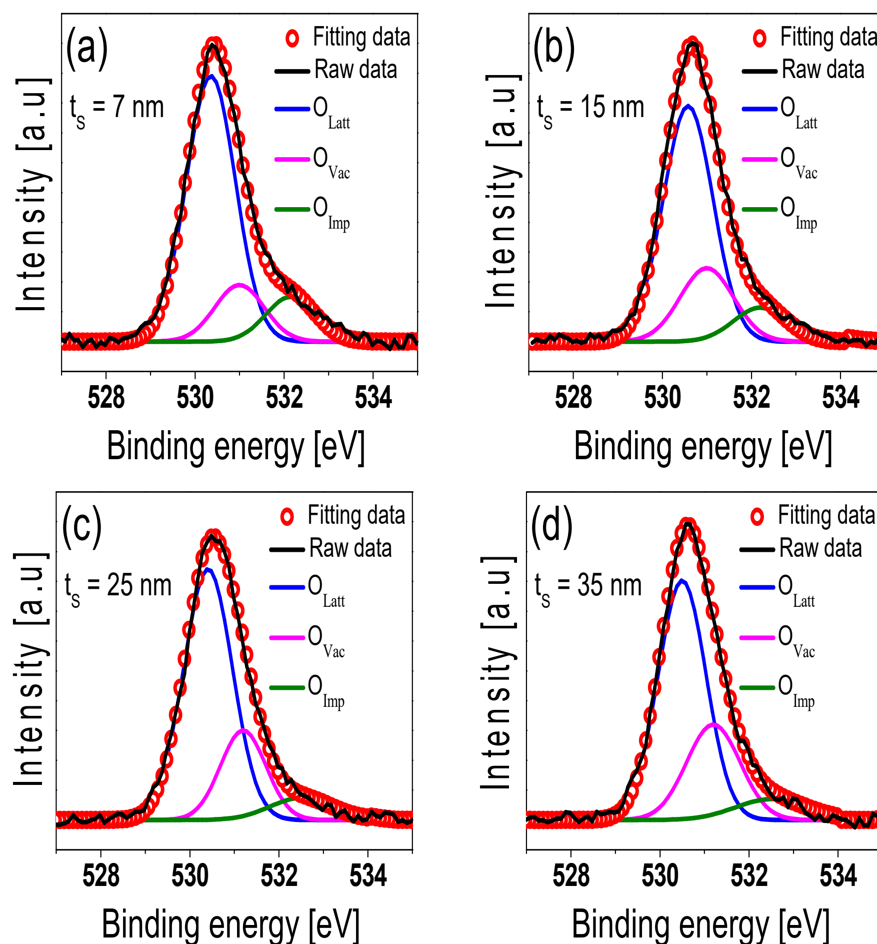

Figure 6. XPS *O*1*s* spectra of the (**a**) 7-nm, (**b**) 15-nm, (**c**) 25-nm, and (**d**) 35-nm thick IGTO thin films located near the IGTO/SiO_2 interface.

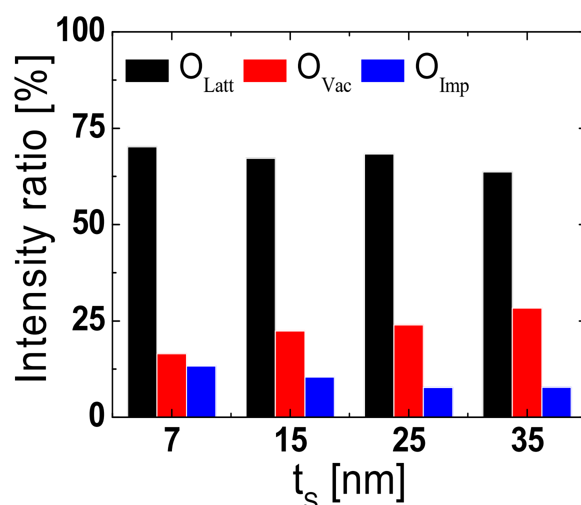

Figure 7. Relative peak area ratios of O_{Latt}, O_{Vac}, and O_{Imp} for the IGTO thin films with different t_S located near the IGTO/SiO_2 interface.

Figure 7 also shows that the relative peak area ratio of O_{Vac} is the smallest for the 7-nm thick IGTO thin film, and it increases with an increase in t_S. O_{Vac} are easily created by sputtering-induced damage in oxide semiconductors [27,36]. Therefore, the concentration of O_{Vac} in IGTO increases with an increase in t_S because of the longer sputtering time. O_{Vac} generates shallow and deep donor states in oxide semiconductors such as IGZO and IGTO [37,38]. Under NBIS, O_{Vac} is ionized to ${O_{Vac}}^{2+}$, and ${O_{Vac}}^{2+}$ drifts toward the oxide semiconductor/gate dielectric interface in oxide TFTs [39]. The increased concentration of electrons, and the formation of an ${O_{Vac}}^{2+}$ accumulation layer near the gate, dielectric shifts the transfer curves of the TFTs in the negative direction [40]. The obtained results show that the lower NBIS stability of the IGTO TFTs with thicker active layers can possibly be attributed to the higher concentration of O_{Vac} in the IGTO thin film, caused by the more severe sputtering-induced damage. The experimental results shown in Figures 4 and 5 indicate that it is necessary to consider the trade-off between the PBS and NBIS stability of the devices, while determining the optimum t_S for IGTO TFTs. From the transfer characteristics and PBS/NBIS stability of the IGTO TFTs with different t_S, it can be concluded that 15 nm is the optimal t_S for IGTO TFTs, leading to the best electrical characteristics (μ_{FE}: 26.5 $cm^2/V{\cdot}s$; *SS*: 0.16 V/dec; and V_{TH}: 0.3 V), and decent PBS and NBIS stability of IGTO TFTs.

4. Conclusions

In this study, we examined the effects of t_S on the transfer characteristics and stability of high-mobility amorphous IGTO TFTs with t_S values of 7, 15, 25, 35, and 50 nm. The obtained results showed that with an increase in t_S, V_{TH} shifted in the negative direction, and the *SS* and μ_{FE} of the fabricated IGTO TFTs increased. Clearly, the PBS stability of the IGTO TFTs improved as the t_S increased. However, the NBIS stability of the IGTO TFTs deteriorated with an increase in t_S. The XPS characterization results revealed that the better PBS stability and the low NBIS stability of the IGTO TFTs with thicker active layers were mainly owing to the decrease in the concentration of OH and the increase in the number of O_{Vac} in the IGTO, with an increase in t_S. We found that the optimum thickness of the active layer for the IGTO TFTs is approximately 15 nm, which results in a positive V_{TH}, an acceptably high μ_{FE}, and decent PBS and NBIS stability of the IGTO TFTs.

Author Contributions: Conceptualization, D.-H.K., H.-S.C. and H.-I.K.; experiment, H.-S.J., H.-S.C. and S.-H.H.; data analysis, D.-H.K. and H.-I.K., writing—original draft preparation, D.-H.K.; supervision, H.-I.K.; and writing—review and editing, H.-I.K. All authors have read and agreed to the published version of the manuscript.

Funding: This research was supported by the National Research Foundation of Korea (NRF) grant funded by the Korean government (MSIT) (No. 2019M3F3A1A03079821) and the Chung-Ang University Research Scholarship Grants in 2017. The authors would like to thank Dr. Shinhyuk Kang (Samsung Corning Advanced Glass) for providing the IGTO sputter target for this study.

Conflicts of Interest: The authors declare no conflict of interest.

References

1. Nomura, K.; Ohta, H.; Takagi, A.; Kamiya, T.; Hirano, M.; Hosono, H. Room-temperature fabrication of transparent flexible thin-film transistors using amorphous oxide semiconductors. *Nature* **2004**, *432*, 488–492. [CrossRef]
2. Fortunato, E.; Barquinha, P.; Martins, R. Oxide semiconductor thin-film transistors: A review of recent advances. *Adv. Mater.* **2012**, *24*, 2945–2986. [CrossRef] [PubMed]
3. Kamiya, T.; Hosono, H. Material characteristics and applications of transparent amorphous Oxide semiconductors. *NPG Asia Mater.* **2010**, *2*, 15–22. [CrossRef]
4. Jang, J.T.; Ahn, G.H.; Choi, S.-J.; Kim, D.M.; Kim, D.H. Control of the boundary between the gradual and abrupt modulation of resistance in the schottky barrier tunneling-modulated amorphous Indium-Gallium-Zinc-Oxide memristors for neuromorphic computing. *Electronics* **2019**, *8*, 1087. [CrossRef]
5. Park, J.-S.; Maeng, W.-J.; Kim, H.-S.; Park, J.-S. Review of recent developments in amorphous Oxide semiconductor thin-film transistor devices. *Thin Solid Films* **2012**, *520*, 1679–1693. [CrossRef]
6. Kikuchi, Y.; Nomura, K.; Yanagi, H.; Kamiya, T.; Hirano, M.; Hosono, H. Device characteristics improvement of a-In–Ga–Zn–O TFTs by low-temperature annealing. *Thin Solid Films* **2010**, *518*, 3017–3021. [CrossRef]
7. Rahaman, A.; Jeong, H.; Jang, J. A High-Gain CMOS Operational Amplifier Using Low-Temperature Poly-Si Oxide TFTs. *IEEE Trans. Electron Devices* **2020**, *67*, 524–527. [CrossRef]
8. Jeong, D.Y.; Chang, Y.; Yoon, W.G.; Do, Y.; Jang, J. Low-Temperature Polysilicon Oxide Thin-Film Transistors with Coplanar Structure Using Six Photomask Steps Demonstrating High Inverter Gain of 264 V V−1. *Adv. Eng. Mater.* **2020**, *22*, 1901497. [CrossRef]
9. Kim, S.-C.; Jeon, Y.-W.; Kim, Y.-S.; Kong, D.-S.; Jung, H.-K.; Bae, M.-K.; Lee, J.-H.; Ahn, B.-D.; Park, S.-Y.; Park, J.-H.; et al. Impact of oxygen flow rate on the instability under positive bias stresses in DC-sputtered amorphous InGaZnO thin-film transistors. *IEEE Electron Device Lett.* **2012**, *33*, 62–64. [CrossRef]
10. Yabuta, H.; Sano, M.; Abe, K.; Aiba, T.; Den, T.; Kumomi, H.; Nomura, K.; Kamiya, T.; Hosono, H. High mobility thin-film transistor with amorphous InGaZnO4 channel fabricated by room temperature rf magnetron sputtering. *Appl. Phys. Lett.* **2006**, *89*, 112123. [CrossRef]
11. Fan, C.L.; Tsao, H.Y.; Chen, C.Y.; Chou, P.C.; Lin, W.Y. New Low-Voltage Driving Compensating Pixel Circuit Based on HighMobility Amorphous Indium-Zinc-Tin-Oxide Thin-Film Transistors for High-Resolution Portable Active-Matrix OLED Displays. *Coatings* **2020**, *10*, 1004. [CrossRef]
12. Fuh, C.-S.; Liu, P.-T.; Huang, W.-H.; Sze, S.M. Effect of annealing on defect elimination for high mobility amorphous Indium-Zinc-Tin-Oxide thin-film transistor. *IEEE Electron Device Lett.* **2014**, *35*, 1103. [CrossRef]
13. Paine, D.-C.; Yaglioglu, B.; Beiley, Z.; Lee, S.-H. Amorphous IZO-based transparent thin film transistor. *Thin Solid Films* **2008**, *516*, 5894–5898. [CrossRef]
14. Ruan, D.-B.; Liu, P.-T.; Chiu, Y.-C.; Kan, K.-Z.; Yu, M.-C.; Chien, T.-C.; Chen, Y.-H.; Kuo, P.-Y.; Sze, S.-M. Investigation of low operation voltage InZnSnO thin-film transistors with dierent high-k gate dielectric by physical vapor deposition. *Thin Solid Films* **2018**, *660*, 885–890. [CrossRef]
15. Noh, J.-Y.; Kim, H.; Nahm, H.-H.; Kim, Y.-S.; Kim, D.H.; Ahn, B.-D.; Lim, J.-H.; Kim, G.H.; Lee, J.-H.; Song, J. Cation composition effects on electronic structures of In-Sn-Zn-O amorphous semiconductors. *J. Appl. Phys.* **2013**, *113*, 3706-1–3706-7. [CrossRef]
16. Kim, B.K.; On, N.; Choi, C.H.; Kim, M.J.; Kang, S.; Lim, J.H.; Jeong, J.K. Polycrystalline Indium Gallium Tin Oxide Thin-Film Transistors With High Mobility Exceeding 100 $cm^2/V{\cdot}s$. *IEEE Electron Device Lett.* **2021**, *42*, 347–357. [CrossRef]
17. Jeong, H.-S.; Cha, H.S.; Hwang, S.H.; Kwon, H.-I. Effects of annealing atmosphere on electrical performance and stability of high-mobility Indium-Gallium-Tin Oxide thin-film transistors. *Electronics* **2020**, *9*, 1875. [CrossRef]
18. Hur, J.-S.; Kim, J.-O.; Kim, H.-A.; Jeong, J.-K. Stretchable polymer gate dielectric by ultraviolet-assisted Hafnium Oxide doping at low temperature for high-performance Indium Gallium Tin Oxide transistors. *ACS Appl. Mater. Interfaces* **2019**, *11*, 21675–21685. [CrossRef] [PubMed]
19. Kim, J.-O.; Hur, J.-S.; Kim, D.-S.; Lee, B.-M.; Jung, J.-M.; Kim, H.-A.; Chung, U.-J.; Nam, S.-H.; Hong, Y.T.; Park, K.-S.; et al. Network structure modification-enabled hybrid polymer dielectric film with Zirconia for the stretchable transistor applications. *Adv. Funct. Mater.* **2020**, *30*, 1906647. [CrossRef]
20. Cho, E.N.; Kang, J.H.; Yun, I. Effects of channel thickness variation on bias stress instability of InGaZnO thin-film transistors. *Microelectron. Reliab.* **2011**, *51*, 1792–1795. [CrossRef]
21. Yang, Z.; Yang, J.; Meng, T.; Qu, M.; Zhang, Q. Influence of channel layer thickness on the stability of amorphous indium zinc oxide thin film transistors. *Mater. Lett.* **2016**, *166*, 46–50. [CrossRef]
22. Lee, S.Y.; Kim, D.H.; Chong, E.; Jeon, Y.W.; Kim, D.H. Effect of channel thickness on density of states in amorphous InGaZnO thin film transistors. *Appl. Phys. Lett.* **2011**, *98*, 122105-1–122105-3. [CrossRef]

23. Li, G.T.; Yang, B.R.; Liu, C.; Lee, C.Y.; Tseng, C.Y.; Lo, C.C.; Lien, A.; Deng, S.Z.; Shieh, H.P.D.; Xu, N.S. Positive gate bias instability alleviated by self-passivation effect in amorphous InGaZnO thin-film transistors. *J. Phys. D Appl. Phys.* **2015**, *48*, 475107. [CrossRef]
24. Jung, S.H.; Moon, H.J.; Ryu, M.K.; Cho, K.I.; Bae, B.S.; Yun, E.-J. The effects of high-energy electron beam irradiation on the properties of IGZO thin films prepared by rf magnetron sputtering. *J. Ceram. Process. Res.* **2012**, *13*, s246–s250.
25. Shin, M.-G.; Hwang, S.-H.; Cha, H.-S.; Jeong, H.-S.; Kim, D.-H.; Kwon, H.-I. Effects of proton beam irradiation on the physical and chemical properties of IGTO thin films with different thicknesses for thin-film transistor applications. *Surf. Interfaces* **2021**, *23*, 100990. [CrossRef]
26. Barquinha, P.; Pimentel, A.; Marques, A.; Pereira, L.; Martins, R.; Fortunato, E. Influence of the semiconductor thickness on the electrical properties of transparent TFTs based on indium zinc oxide. *J. Non-Cryst. Solids* **2006**, *352*, 1749–1752. [CrossRef]
27. Li, J.; Ding, X.W.; Zhang, J.H.; Zhang, H.; Jiang, X.Y.; Zhang, Z.L. Improving electrical performance and bias stability of HfInZnO-TFT with optimizing the channel thickness. *AIP Adv.* **2013**, *3*, 102132. [CrossRef]
28. Park, H.-W.; Park, K.; Kwon, J.-Y.; Choi, D.; Chung, K.-B. Effect of active layer thickness on device performance of tungsten-doped InZnO thin-film transistor. *IEEE Trans. Electron Dev.* **2016**, *64*, 159–163. [CrossRef]
29. Wang, Y.; Sun, X.W.; Goh, G.K.L.; Demir, H.V.; Yu, H.Y. Influence of Channel Layer Thickness on the Electrical Performances of Inkjet-Printed In-Ga-Zn Oxide Thin-Film Transistors. *IEEE Trans. Electron. Dev.* **2011**, *58*, 480–485. [CrossRef]
30. Nguyen, C.P.T.; Raja, J.; Kim, S.; Jang, K.; Le, A.H.T.; Lee, Y.-J.; Yi, J. Enhanced electrical properties of oxide semiconductor thin-film transistors with high conductivity thin layer insertion for the channel region. *Appl. Surf. Sci.* **2014**, *396*, 1472–1477. [CrossRef]
31. Lee, E.; Kim, T.H.; Lee, S.W.; Kim, J.H.; Kim, J.; Jeong, T.G.; Ahn, J.-H.; Cho, B. Improved Electrical Performance of a Sol-Gel IGZO Transistor with High-k Al2O3 Gate Dielectric Achieved by Post Annealing. *Nano Converg.* **2019**, *6*, 1–8. [CrossRef] [PubMed]
32. Ji, H.; Hwang, A.Y.; Lee, C.K.; Yun, P.S.; Bae, J.U.; Park, K.-S.; Jeong, J.K. Improvement in Field-Effect Mobility of Indium Zinc Oxide Transistor by Titanium Metal Reaction Method. *IEEE Trans. Electron Devices* **2015**, *62*, 1009–1013.
33. Kumaran, S.; Liu, M.-T.; Lee, K.-Y.; Tai, Y. The Impact of Solvents on the Performances of Solution-Processed Indium Gallium Zinc Oxide Thin-Film Transistors Using Nitrate Ligands. *Adv. Eng. Mater.* **2020**, *22*, 1901053. [CrossRef]
34. Kim, S.T.; Shin, Y.; Yun, P.S.; Bae, J.U.; Chung, I.J.; Jeong, J.K. Achieving High Carrier Mobility Exceeding 70 $cm^2/V{\cdot}s$ in Amorphous Zinc Tin Oxide Thin-Film Transistors. *Electron. Mater. Lett.* **2017**, *13*, 406–411. [CrossRef]
35. Mativenga, M.; Um, J.G.; Jang, J. Reduction of Bias and Light Instability of Mixed Oxide Thin-Film Transistors. *Appl. Sci.* **2017**, *7*, 885. [CrossRef]
36. Khan, S.A. Amorphous Metal-Oxide Based Thin Film Transistors on Metal Foils: Materials, Devices and Circuits Integration. Ph.D. Thesis, Deptartment Electrical Engineering, University Lehigh, Bethlehem, PA, USA, 2018.
37. Jeong, H.-J.; Lee, H.-M.; Oh, K.-T.; Park, J.; Park, J.-S. Enhancement of In–Sn–Ga–O TFT performance by the synergistic combination of UV + O_3 radiation and low temperature annealing. *J. Electroceram.* **2016**, *37*, 158–162. [CrossRef]
38. Kamiya, T.; Nomura, K.; Hirano, M.; Hosono, H. Electronic structure of oxygen deficient amorphous oxide semiconductor a-InGaZnO4–x: Optical analyses and first-principle calculations. *Phys. Stat. Sol.* **2008**, *5*, 3098–3100.
39. Kim, J.H.; Park, E.-K.; Kim, M.S.; Cho, H.J.; Lee, D.-H.; Kim, J.-H.; Khang, Y.; Park, K.; Kim, Y.-S. Bias and illumination instability analysis of solution-processed a-InGaZnO thin-film transistors with different component ratios. *Thin Solid Films* **2018**, *645*, 154–159. [CrossRef]
40. Oh, H.; Yoon, S.M.; Ryu, M.K.; Hwang, C.S.; Yang, S.; Park, S.H. Photon-accelerated negative bias instability involving subgap states creation in amorphous In–Ga–Zn–O thin film transistor. *Appl. Phys. Lett.* **2010**, *97*, 183502. [CrossRef]